Water-based processing of $LiFePO_4$ positive electrodes for Li-ion batteries: effect of particle size and active material loading on the performance of the electrodes

Berke Karaman[1], Luis D. Couto[2], Mohammad Chargkhgard[3], Michel Kinnaert[3], Nathalie Job*[1]

[1] *University of Liège, Department of Chemical Engineering - NCE (Nanomaterials, Catalysis, Electrochemistry), 4000 Liège, Belgium*
[2] *Vlaamse Instelling voor Technologisch Onderzoek (VITO), Unit Energy Technology, B-2400 Mol, Belgium*
[3] *Université Libre de Bruxelles, Department of Control Engineering and System Analysis, 1050 Brussels, Belgium*

*(*corresponding author: Nathalie.Job@uliege.be)*

Abstract

$LiFePO_4$ (LFP) powders with 0.84 µm and 0.24 µm average particle sizes are studied as Li-ion battery materials using a water-based electrode manufacturing process. Along with the compatibility with aqueous processing, the impact of particle size and active material loading on the performance of the electrodes is studied, especially in terms of capacity, rate capability and stability. Decrease of rate capability and capacity with increasing electrode loading is observed for both cases due to increase of internal resistance with increasing electrode loading. However, the LFP with lower particle size is much less affected by the increase of electrode loading due to considerably lower charge transfer resistance at the material surface. Degradation upon cycling highly depends on the electrode loading, the phenomenon being more and more acute as the electrode loading goes from 1.6 to 6.4 mg/cm². Degradation is due to the increase of both internal resistance and charge transfer resistance; however, it is pointed out that degradation is lessened by decreasing the LFP particle size. In conclusion, both the material morphology and the electrode design have to be taken into account for electrode manufacturing.

Keywords: Li-ion batteries, LFP, water-based electrode manufacturing, particle size, electrode loading

1. Introduction

In the current evolution of the world, the energy demand increases year by year, which calls for better resource management. To change direction towards a more sustainable world, the electrical energy generated by solar, wind and other renewable sources needs to be stored and used more efficiently. Electrochemical storage devices are thus key technologies. For that purpose, along with other systems, Li-ion batteries are one of the most popular energy storage devices due to their high energy and power density [1]. However, since a battery is made of several components, various design selections should be considered in the production process of the batteries, depending among others on the final use. The main components of the battery cells are the electrolyte, the electrodes (including current collectors) and the separator. Among these, it must be pointed out that electrodes are usually composite media, including (i) the active material that stores Li^+ ions, (ii) binders, (ii) conductive additives, all having an impact on the cell properties; thus, the design of the electrode is highly important.

First, the selection of the electrode active material among various options is crucial. In the case of the positive electrode, Lithium Cobalt Oxide (LCO) remains very common due to its high insertion/deinsertion potential (~4 V *vs.* Li^+/Li), which results in high energy density cells when coupled to, *e.g.*, graphite as negative electrode material (insertion/deinsertion potential ~0.5 V *vs.* Li^+/Li). However, due to high cost, as well as availability and safety issues associated with cobalt, NMC (*i.e.* $LiNi_{1-y-z}Mn_yCo_zO_2$) are progressively taking the lead. To fully eliminate Co, other active materials are also currently considered [1,2]. Among those, $LiFePO_4$ (LFP) is one of the most popular positive electrode materials for Li-ion batteries due to its increased safety, abundancy of precursor materials and relatively high capacity [3]. However, LFP displays relatively low density, poor electronic conductivity and low ionic diffusivity [4].

Second, the design of the electrode from its components must be carefully considered. In particular, the active material must be blend with a binder in a solvent to finally be deposited (usually by blade casting) onto a metallic current collector, the final electrode being obtained after solvent elimination. Although current processes still use polyvinylidene difluoride (PVDF) and N-methyl-pyrrolidone (NMP) as binder and solvent, respectively, it appears more and more necessary to move towards water-based suspensions for both economic and environmental reasons. In that field, Na-CMC-styrene-butadiene rubber combinations (CMC

standing for carboxymethylcellulose) have been widely used for aqueous formulation of electrodes [5]. Alternatively, in previous works [6,7], our research group developed a water-based spray-coating process using xanthan gum, which proved efficient to manufacture cells with both LFP and $Li_4Ti_5O_{12}$ (LTO), in half cell and full cell configurations, with different amounts of active materials as well as different current collectors. Comparison with traditional PVDF/NMP was conducted and identical performance were obtained, proving XG/water is a viable candidate to replace PVDF/NMP.

Coming back to the active material, its chemical nature is not the only parameter to be considered. Given that electrodes are prepared from powders, the active material granulometry has an impact on both the manufacturing process and on the final electrode properties [8,9] given that the Li^+ ions have to diffuse within those particles during insertion/deinsertion. For example, Sinha *et al.* [10] explain in a review how the particle size of the widely used positive electrode materials powders (such as LCO, LFP, Lithium Manganese Oxide - LMO, *etc.*) affects the performance of the cells. The coating thickness also has an impact due to electron and ion conductivity limitations within the active material and the electrolyte. As an example, in a study that focuses on the impact of the electrode thickness on the electrochemical and thermal characteristics of Li-ion batteries, Zhao *et al.* [11] concluded that the thicker electrodes release more heat by ohmic effect at the same discharge rate compared to thinner ones. Additionally, those parameters affect diffusion distances and concentration polarization, both having high impacts on the performance of the cells. Therefore, such parameters must be controlled and chosen carefully to meet the expectations in terms of performance and stability of the battery.

More specifically, with regard to LFP electrodes, a detailed study by Logan *et al.* [12] focused on how the specific surface area and the particle size of the LFP powder affect the cell aging; it concluded that, after long-term cycling, LFP particles with large size display micro-fractures and lose their storage capacity. In another paper, the impact of the particle size distribution on the rate capability of the electrodes was studied by Zhang *et al.* [13]. The results show that broader particle size distribution of the LFP powders offers better pathways for electron transport and reduces the contact resistance, hence improving the rate capability of the cells. Although many studies focused on different design parameters, works considering the joint impact of both the powder particle size and the electrode loading are less common, especially when water-based formulations are considered.

The aim of the present study is to link the effects of the LFP particle size and electrode loading with the performance and stability of LFP electrodes manufactured using a water-based process. In particular, it aims at understanding how the impacts of those two design parameters can compensate each other. To that aim, electrodes with two different LFP particle sizes and various electrode loadings were prepared. The electrodes were assembled in half-cells and their performance and stability were studied by galvanostatic charge-discharge method. Electrochemical impedance spectroscopy was also performed to understand the origin of the performance and stability differences observed. The whole study was performed on electrodes prepared *via* the process previously developed at the laboratory, *i.e.* spray-coating of a water-based electrode formulation using xanthan gum as a binder. The obtained results show a clear impact of the particle size on the electrode performance, and allow to define electrode loading limits with regard to the expected performance at high cycling speed.

2. Experimental

2.1. Preparation of electrodes

Two different $LiFePO_4$ (LFP) powders were selected for this study: P700 and P800 from Prayon/PuLead and referred to as LFP-1 and LFP-2 hereafter. Following the manufacturer, the two materials are carbon-coated (1.3 wt.) to enhance electron conductivity. The powders were characterized and used as received. Electrodes were produced *via* robotic spray coating of a water-based suspension by adapting a previously published method [6] where manual airbrush was used. The aqueous suspension, prepared in MilliQ water, contained 12 wt% solids including LFP, xanthan gum (Sigma-Aldrich) and conductive additive (carbon black Timcal C-nergy Super C65) in a weight ratio of 75:20:5 (active material:conducting carbon:binder). The mixture was stirred at room temperature with a magnetic stirrer for 3 h prior to electrode manufacturing. The prepared ink was sprayed onto pre-weighted stainless-steel discs current collectors (type 304, ∅ = 15.5 mm, MTI corp.) and dried overnight at 60°C under air in an oven. Different LFP loadings were prepared: 3 mg (1.59 mg/cm^2), 6 mg (3.17 mg/cm^2) and 12 mg (6.35 mg/cm^2). The coated discs were then weighted and dried again in an oven for 2 h under vacuum (2000 Pa) at 110°C before being introduced into the glovebox. The half-cells were assembled using LFP electrode as positive electrode, metallic Li disc (PI-KEM) as counter and reference electrode, two Celgard® separators and 80 µL of electrolyte (1 M $LiPF_6$ in an ethylene carbonate:diethyl carbonate:dimethylcarbonate – 1:1:1 mixture, Sigma Aldrich).

Prepared half-cells were then used for electrochemical characterization. Note that the pH of both slurries (containing either P700 or P800) was measured equal to 8.8 and 9.2 for P700 and P800 slurries, respectively. This observation rules out any current collector corrosion issue, 304 SS being quite stable under those conditions [14]. Also, taking into account the very fast drying time of the coating upon spray drying (a few seconds), this slurry composition should not bring any issue either should Al be used instead of SS [15], as already observed in our previous study [6].

2.2. Characterization

2.2.1. Physico-chemical characterization

The LFP powders were analysed by nitrogen adsorption-desorption. The isotherms were measured at -196°C using a Micromeritics ASAP 2420 automatic device (Micromeritics, Norcross, USA). The samples were degassed overnight at 270°C under vacuum (133 Pa) prior to the measurements. The specific surface area, A_{BET}, was calculated using the Brunauer-Emmett-Teller (BET) equation, the adsorption data being taken in the adequate range of relative pressure (P/P_0), accounting for the Rouquerol criterion. Scanning electron microscopy (SEM) images were obtained on a FEG-SEM Tescan CLARA at 15 kV under high vacuum conditions. The samples were coated with a 15-nm gold layer by sputtering and mounted with carbon adhesive prior to observation.

2.2.2. Electrochemical characterization

LFP half-cells were characterized using a BioLogic VMP3 multichannel potentiostat. Prior to any electrochemical test, cells were first submitted to formation cycles between 2.0 and 4.2 V *vs.* Li^+/Li by using galvanostatic charge and discharge cycling in the following sequence: 10 cycles at C/5 (*i.e.* 5 h of charge and 5 h of discharge) and 10 cycles at C (*i.e.* 1 h of charge and 1 h of discharge). Then, the overall cell performance was assessed by performing 10 cycles at C/5, C/2, C, 2C, 5C. Finally, to compare the stability of the cells, 100 cycles of galvanostatic charge-discharge cycles at C were added and the cycling finalized with a second performance assessment sequence including again 10 cycles at C/5, C/2, C, 2C, 5C. Cells were compared according to their capacities at given C-rates and capacity retention after long-term cycling.

Note that all applied current densities were calculated considering a theoretical capacity of 170 mAh/g for LFP [16].

Electrochemical impedance spectroscopy (EIS) was conducted with the same device in the 10^{-2} - 10^{6} Hz frequency range at 25°C. Apart from the frequency range, the State Of Charge (SOC) level of the cells greatly affects the results of EIS spectra; therefore, its value should be chosen beforehand. According to literature, SOC levels were selected separately for performance and stability investigations. Indeed, in earlier studies, it has been observed that EIS spectra differences are more apparent at 100% SOC for stability investigations [17]; the same SOC was thus chosen for stability studies. For performance investigations, SOC was fixed as 40% since it has been stated in literature that limit potentials, compared to mid potentials, leads to higher polarization, possibly due to side reactions [18]. EIS was performed after the formation cycles and at the end of the second performance cycling sequence to highlight the impact of aging on the electrode properties.

3. Results and discussion

3.1. Physico-chemical characterization of the LFP powders

LFP powders were first observed by SEM (Figure 1) to check their morphology and determine their particle size distribution. LFP-1 is constituted of particles of very variable size (Figure 1a) while LFP-2 displays a much more homogeneous structure (Figure 1b). A minimum of 90 particles were randomly selected and their diameter measured manually to calculate the mean particle size (along with its standard deviation, σ) of both samples (Figure 2). Values were

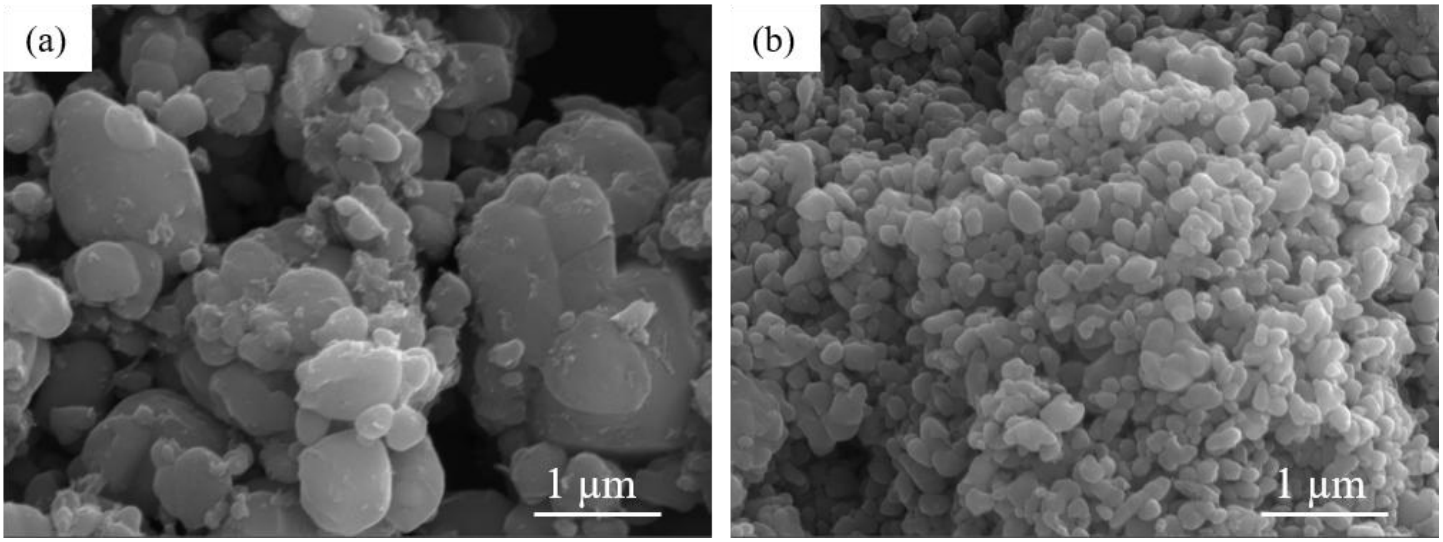

Figure 1. Representative examples of SEM images of (a) LFP-1 and (b) LFP-2 powders.

calculated equal to 0.84 and 0.26 µm for LFP-1 and LFP-2 powders, respectively. The corresponding standard deviations, σ, equal 0.45 and 0.26 µm, meaning that LFP-2 presents smaller particles with much narrower size distribution than LFP-1.

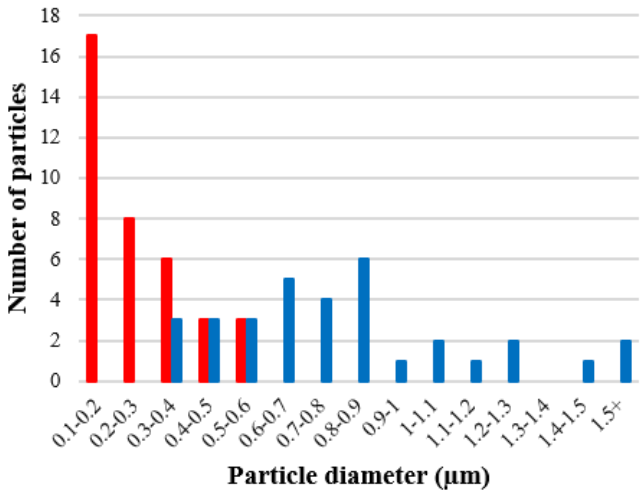

Figure 2. Particle size distribution of LFP-1 (—) and LFP-2 (—) powders observed *via* SEM.

The two powder samples were characterized by N_2 adsorption-desorption technique to determine their specific surface areas. Values calculated by the BET method, A_{BET}, were found to be 10.7 m^2/g and 13.1 m^2/g for LFP-1 and LFP-2, respectively. Those surfaces much certainly correspond to the external surface of LFP particles: indeed, the adsorption isotherms (Figure 3) correspond to a type II isotherm (non-porous or microporous material) following IUPAC's classification. Although those values do not seem to be very different, it has been noted in several studies that such a discrepancy is significant enough to impact the performances of Li-ion battery electrodes [12,19].

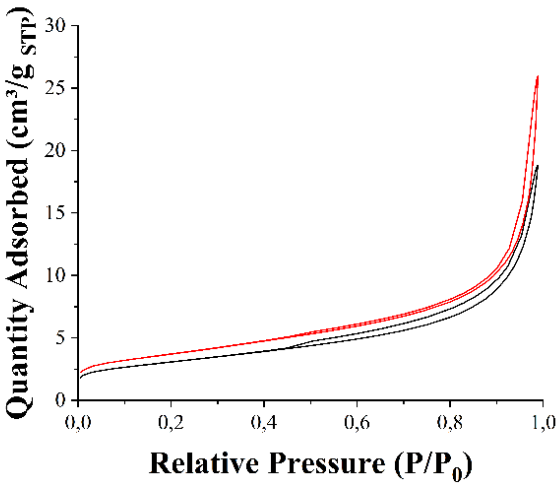

Figure 3. N_2 adsorption-desorption isotherms of the LFP-1 (—) and LFP-2 (—) powders.

3.2. Electrode performance

Galvanostatic charge and discharge was performed to determine the electrode capacity retention as a function of both the electrode thickness (*i.e.* the LFP loading) and cycling rate. The results are compared according to the LFP loading of the electrodes (Figure 4).

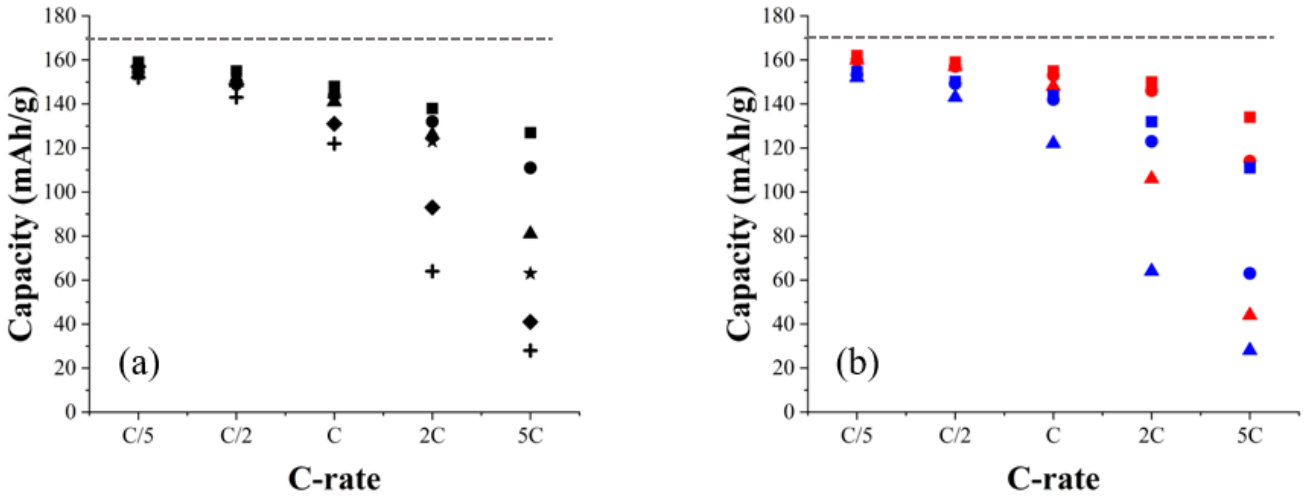

Figure 4. (a) Comparison of LFP-1 electrodes capacity *vs.* C-rate as a function of the LFP loading. (■) Below 2 mg, (●) 2-4 mg, (▲) 4-6 mg, (★) 6-8 mg, (♦) 8-10 mg, (+) 12 mg. (b) Comparison of LFP-1 (—) and LFP-2 (—) electrode *vs.* C-rate as a function of the loading on the electrodes; 3 mg (■), 6 mg (●), 12 mg (▲). The dashed line on both figures represents the theoretical capacity of LFP. Measurements performed at 25°C.

Table 1 shows all the data obtained from the experiments performed on electrodes of various loadings prepared with samples LFP-1. Firstly, it was aimed at observing the direct effect of material loading on the capacity of the electrodes. In order to do that, a wide range of LFP-1 loadings starting from below 2 mg up to 12 mg has been selected and minimum of 2 cells used each time. Then, in order to observe how the particle size affects phenomena observed with LFP-1 electrodes of various loadings, a second set of charge-discharge tests was performed with LFP-2. For the sake of simplicity of comparison, electrodes prepared with loadings around 3 mg (±0.5 mg), 6 mg (±0.5 mg) and 12 mg (±0.5 mg) have been used. Those selected electrodes are noted as 3 mg, 6 mg and 12 mg LFP loading electrodes from now on for simpler notation. Results are gathered in Table 2. In that table, the values indicated are the average values obtained on at least 3 cells displaying LFP loadings within the mentioned range.

Table 1. Average capacities of the LFP-1 electrodes with various LFP loading at various cycling speed.

	Capacity[b] (mAh/g)				
LFP loading[a] (mg)	**C/5**	**C/2**	**C**	**2C**	**5C**
< 2	159 (±2)	155 (±3)	148 (±2)	138 (±2)	127 (±5)
2-4	154 (±5)	150 (±2)	144 (±2)	132 (±1)	111 (±6)
4-6	154 (±2)	150 (±2)	141 (±2)	126 (±5)	81 (±8)
6-8	153 (±1)	149 (±4)	142 (±6)	123 (±10)	63 (±10)
8-10	158 (±2)	150 (±2)	134 (±3)	91 (±6)	41 (±9)
10-12	153 (±3)	144 (±1)	124 (±4)	71 (±7)	34 (±8)

[a] Range of loading for the LFP-1 electrodes considered. [b] Average capacity on at least 3 cells.

In the case of LFP-1 (Table 1), for all electrodes, the capacity observed at a low C-rate (C/5) is very similar (153 – 159 mAh/g), even though it slightly decreases with increasing loading. At low loading (below 2 mg), the capacity also decreases from 159 to 127 mAh/g when increasing the C-rate from C/5 to 5C. Capacity decrease is observed for all electrode loadings. As expected, it gets more pronounced as the LFP loading increases and is especially dramatic for the high C-rates: at 5C and for the highest LFP loading, the difference is about 100 mAh/g compared to the lowest loading. The reasons of the decrease in capacity at high C rates can be

explained by charge transport limitation within the electrode: as the electrode gets thicker, charge transport across the electrode gets more difficult, which explains the change in observed electrochemical properties.

As indicated above, LFP-2 half-cells were characterized in the same way to highlight the effect of the material particle size on the performance of the battery (Figure 4b). The obtained capacities are reported in Table 2, along with those of LFP-1 with similar LFP loadings. Firstly, one observes that the rate capability (*i.e.* electrode ability to accommodate different C-rates) of LFP-2 is significantly different from that of LFP-1. When comparing the 3 mg LFP coatings, the capacity at 5C drops to 67% of that observed at C/5 in the case of LFP-1. By comparison, LFP-2 can sustain up to 85% of its capacity when the cycling rate increases from C/5 to 5C. Secondly, the drastic capacity difference at high C-rates observed between 12 mg LFP coatings from LFP-1 and LFP-2 shows that LFP-2 electrodes are much less affected by the increase of coating thickness. For LFP-1, the capacity retentions compared to C/5 (considered as 100%) are 94%, 80%, 42% and 18% for C rates of C/2, C, 2C, 5C, respectively. For LFP-2, those values increase to 98%, 92%, 66%, 27% for the same C rates.

Table 2. Average capacities at various cycling speed and resistances of the LFP-1 and LFP-2 electrodes with various LFP loadings.

		Capacity[b] (mAh/g)					Resistance		
	LFP loading[a] (mg)	**C/5**	**C/2**	**C**	**2C**	**5C**	R_0 **(Ω.mg)**	R_i **(Ω.mg)**	R_{ct} **(Ω.mg)**
LFP-1	**3**	155 (±3)	150 (±2)	144 (±1)	131 (±1)	109 (±5)	31	15	93
	6	153 (±1)	151 (±2)	144 (±2)	127 (±6)	75 (±3)	30	32	96
	12	155 (±3)	143 (±6)	125 (±3)	77 (±10)	32 (±7)	32	56	98
LFP-2	**3**	162 (±2)	159 (±1)	158 (±2)	150(±2)	134 (±3)	26	17	53
	6	160 (±2)	156 (±2)	150 (±3)	138 (±9)	96 (±12)	27	40	70
	12	158 (±3)	153 (±6)	148 (±8)	106 (±2)	39 (±5)	29	61	88

[a] Range ± 0.5 mg. [b] Average capacity on at least 2 cells.

The reason for these discrepancies between electrodes prepared either using LFP-1 or LFP-2 was further investigated by Electrochemical Impedance Spectroscopy (EIS). The high frequency region (10 kHz to 1 kHz) and mid frequency region (1 kHz to 1 Hz) of the Nyquist plot is used to quantify interface resistance (R_0), the internal resistance (R_i) and the charge transfer resistance (R_{ct}). Following the literature, R_0 would correspond to the resistance between the coating and the current collector [20] while R_i corresponds to the internal resistance value of the bulk of the electrode, including current collector, active material, electrolyte and separator [21,22]. In the meantime, R_{ct} represents the charge transfer resistance at the electrode/electrolyte interface [21-23]. While the intersection between the EIS spectra and the X-axis corresponds to R_i, R_{ct} is obtained from the radius of the semi-circle in mid-frequency range [24,25].

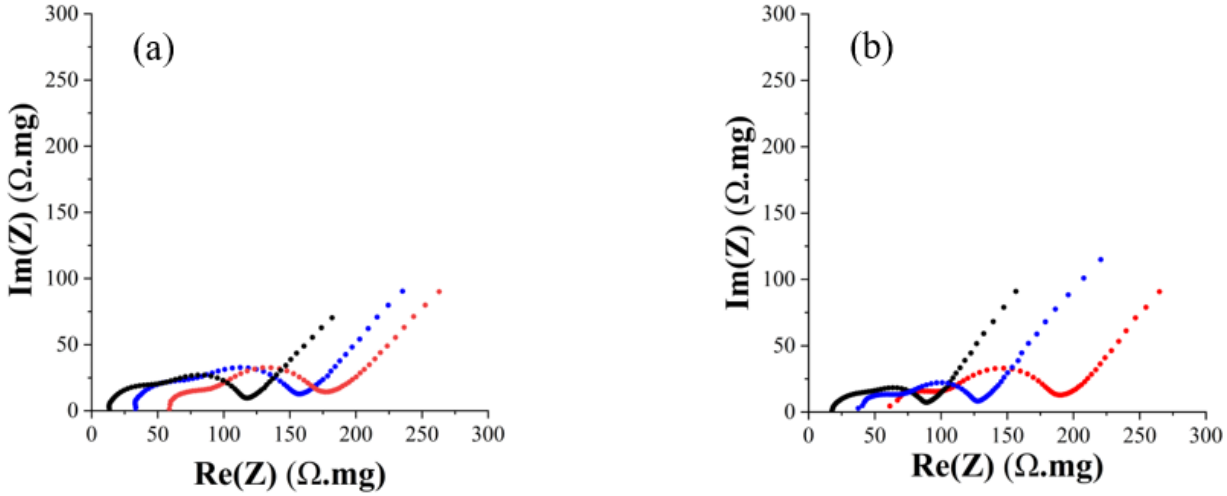

Figure 5. Electrochemical impedance spectra of (a) LFP-1 and (b) LFP-2 cells with LFP loading of 3 mg (●), 6 mg (●), 12 mg (●). Measurements performed at 25°C.

To start with, significant difference in interface resistance R_0 can be observed between LFP-1 and LPF-2, whatever the active material loading. Following this, in the case of the LFP-1 electrodes, R_i is observed equal to 15 Ω.mg, 32 Ω.mg and 56 Ω.mg for 3 mg, 6 mg and 12 mg electrodes, respectively (Figure 5a). In other words, an increase in the internal resistance of the electrode with increasing LFP loading is observed, as expected. When the electrode loading increases, charge transport within the coating becomes more difficult, which is reflected in the EIS spectra as a shift of the semi-circle intersection with the X-axis towards higher values. This phenomenon is also seen in other studies and explains the differences in the electrochemical performance such as capacity, rate capability, *etc.* (Figure 4a) [23,26]. Meanwhile, LFP-2 cells

were also characterized using the same procedure. The same phenomenon is observed: with increasing LFP loading, R_i increases as well. R_i for 3 mg LFP coating is measured equal to 17 Ω.mg while it increases to 40 Ω.mg and 61 Ω.mg for 6 mg and 12 mg LFP coating, respectively (Figure 5b). Therefore, an increase of the internal resistance can be the cause of capacity drop at high C-rates. However, R_{ct} does not change as drastically as R_i: values are determined as 93, 96 and 98 Ω.mg for 3 mg, 6 mg and 12 mg LFP-1 loadings respectively. This observation was expected since the charge transfer resistance depends mainly on the active material particle size [27]. However, more apparent changes can be observed for LFP-2 since the charge transfer resistances are equal to 53, 77 and 88 Ω.mg for 3 mg, 6 mg and 12 mg LFP-2 loadings, respectively. Therefore, one can argue that the advantage of having more surface area with lower particle size fades away with increased electrode loading. The increase of loading, and therefore the increase of coating thickness, possibly leads to a decrease of electrolyte accessibility to the LFP surface.

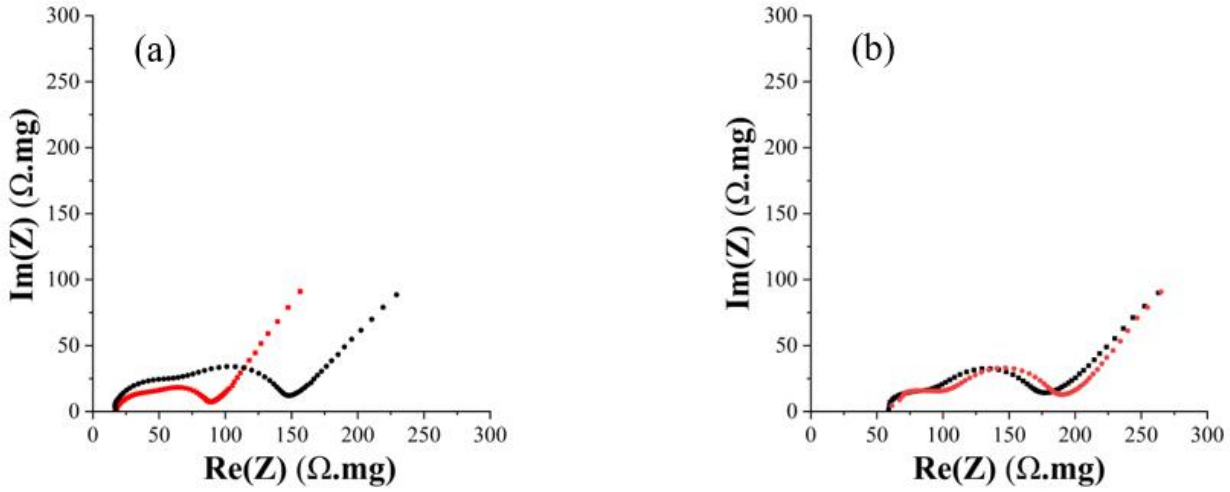

Figure 6. Electrochemical impedance spectra of LFP-1 (●) and LFP-2 (●) for (a) 3 mg LFP and (b) 12 mg LFP. Measurements performed at 25°C.

Following this, LFP-1 and LFP-2 cells are compared (Table 2); for both 3 mg and 12 mg LFP cells, one realizes that the R_i values do not differ much from each other. However, huge differences between R_{ct} values measured on 3 mg LFP electrodes can be observed: indeed, one obtains R_{ct} values of 93 Ω.mg and 53 Ω.mg for LFP-1 and LFP-2, respectively (Figure 6). This is expected as higher surface area offers more area for electrons to transfer, which reduces the

charge transfer resistance [23,26]. Therefore, the better rate capability of the LFP-2 can be explained by reduced charge transfer resistance (Figure 5b). However, when observing the 12 mg LFP electrodes, the difference between charge transfer resistances of LFP-1 and LFP-2 electrodes is much less pronounced: indeed, one obtains 98 and 88 Ω.mg for LFP-1 and LFP-2, respectively. Although a difference is observed between the two different LFP powders, the impact of the particle size gets lower with increasing electrode loading.

3.2. Stability

The electrode stability was studied by galvanostatic charge and discharge method. Electrodes were first submitted to 5 different C-rates (C/5, C/2, C, 2C, 5C) to obtain the results shown previously in Figure 4; then, they underwent 100 cycles at C and, finally, were tested again at the same 5 different C-rates. Results are now compared on the basis of capacity retention at the same C-rates before and after the series of 100 cycles at C. Also, the first 5 cycles of the 100-cycle sequence were compared with the last 5 cycles to quantify the impact of long-term cycling at stable C-rate on the electrode capacity. The stability study was conducted for both LFP-1 and LFP-2 samples and for different LFP loadings (3, 6 and 12 mg). Table 4 gathers the results obtained; those results are presented as the percentage of capacity retention between the two sequences. As an example, the column "C/5" displays the percentage of capacity remaining at C/5 between the two sequences at variable rate, before and after the series of 100 cycles at C. The last column, labelled as "C × 100", corresponds to the capacity retention between the beginning (first 5 cycles) and end (last 5 cycles) of the sequence of 100 cycles at C.

The stability of the electrodes greatly depends on their loading. Whatever the LFP sample chosen, the electrodes with 3 mg of LFP seem to be the most stable at any C-rate while 12 mg LFP electrodes are observed to be the least stable ones. The deviation from that trend, observed at 2C and 5C for 6 mg and 12 mg electrodes, probably comes from the already low capacity values measured at high C-rates.

Table 4. Capacity retention values of LFP-1 and LFP-2 electrodes with various LFP loadings at different C-rates.

		Capacity retention (%)					
	LFP loading[a] (mg)	**C/5**	**C/2**	**C**	**2C**	**5C**	**C × 100[b]**
LFP-1	**3**	95	95	94	92	73	96
	6	92	74	52	36	49	68
	12	84	48	28	42	67	32
LFP-2	**3**	95	94	94	90	81	97
	6	94	89	82	69	53	88
	12	87	56	33	37	68	36

[a] Range ± 0.5 mg. [b] Comparison between the 5 first cycles and the last 5 cycles of the 100-cycle series at C.

Those results show that, although the stability is similar for LFP-1 and LFP-2 with thin electrode coatings, the difference gets quite significant in the case of thicker coatings, *i.e.* with 6 mg and 12 mg loadings. When results obtained with 6 mg LFP coatings are thoroughly examined, significant differences between LFP-1 and LFP-2 can be observed. At 2C especially, the capacity of LFP-1 after the series of 100 cycles at C falls to 36% of the value measured before. By contrast, after long-term cycling, sample LFP-2 can hold 69% of its initial capacity at the same cycling speed. For the 12 mg LFP coatings, a difference between LFP-1 and LFP-2 electrodes is still observed; however, that difference is not as significant as in the case of 6 mg LFP coatings as LFP-1 can hold 66% of its initial capacity while LFP-2 can hold 88%. Therefore, 12 mg LFP coatings in general are not so appropriate regarding stability aspect.

EIS was conducted at the end of the 100-cycle series, using the same procedure as earlier. All resistances, R_0, R_i and R_{ct}, generally increase with electrode aging (Table 5) [28–30]. The R_i increase might be ascribed to phenomena such as microcracks appearance, gas evolution, corrosion of current collector, *etc.* and it is usually difficult to distinguish which one is the main reason without intensive *post mortem* analysis. The above-listed potential physical changes in the electrode could also explain the increase of R_0. Regarding R_{ct}, one can argue that the decrease of total electrode surface due to the decrease of loading results in decreasing the contact surface between the active material and the electrolyte. Therefore, more limited area for charge transfer would result as charge transfer resistance increase [23]. Although increase of resistances by aging of the electrodes has been reported many times in literature, the impact of particle size and electrode loading on this phenomenon is not inspected thoroughly.

However, measurements could not be performed properly for 6 mg and 12 mg electrode groups as the cells were severely damaged by cycling and were not able to provide meaningful EIS signals. Therefore, the comparisons are made between 3 mg electrodes only, for both LFP-1 and LFP-2 samples. In the case of LFP-1, the EIS spectra before and after long-term cycling (Figure 7a) shows obvious differences. The intersection between the EIS curve and the X-axis shifts towards higher values; therefore, R_i increases. In the meantime, the radius of the semi-circle at medium frequencies, which corresponds to R_{ct}, gets bigger. Before long-term cycling, R_i is equal to 16 Ω.mg while, after the 100-cycle sequence, it doubles to 32 Ω.mg (Table 5). Increase of R_i by aging is observed in many studies and can be ascribed to losses of active materials by dissolution of active substances, lithium plating, *etc.* [17,29–31]. A significant increase of R_{ct} is also observed: from 42 to 65 Ω.mg. Therefore, the decrease in capacity and rate capability from the beginning to the end of the testing sequence can be explained by the increase of both resistances.

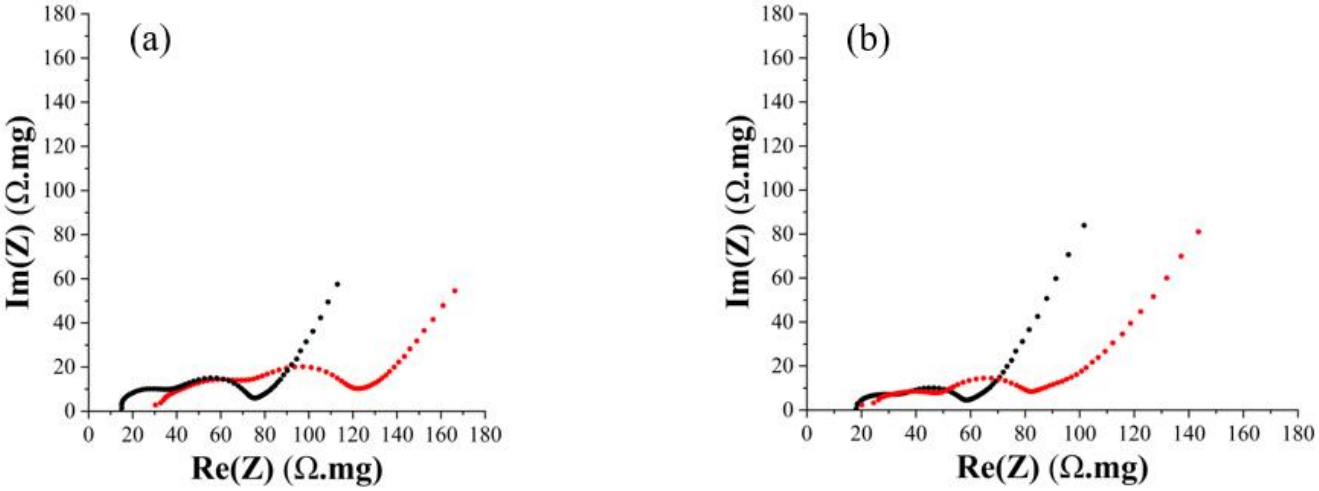

Figure 7. Electrochemical impedance spectra of (a) 3 mg LFP-1 electrodes and (b) 3 mg LFP-2 electrodes before (●) and after (●) cycling. Measurements performed at 25°C.

In the case of LFP-2, EIS measurements conducted on the 3 mg coating (Figure 7b) also show a shift of spectra to X-axis increasing values and an increase of the radius of the semi-circle in the mid-frequency range, but not to the same extent as LFP-1. The value of R_i slightly increases, from 18 to 20 Ω.mg ; however, the charge transfer resistance, R_{ct}, displays the highest increase by going up from 28 to 43 Ω.mg. An increase in charge transfer resistance upon ageing was

observed in other studies [28,32]. However, those works do not highlight the impact of the particle size effect aging phenomena while it is obvious in the present study. Although both 3 mg LFP-1 and 3 mg LFP-2 electrodes show R_i and R_{ct} increases upon aging, the impact is much less pronounced for LFP-2. Small particles are thus much less prone to aging than large ones.

Table 5. Interface resistance, internal resistance and charge transfer resistance of LFP-1 and LFP-2 electrodes with 3 mg LFP loading before and after cycling.

	LFP-1		**LFP-2**	
	Before	After	Before	After
R_0 **(Ω.mg)**	17	35	12	29
R_i **(Ω.mg)**	16	32	18	20
R_{ct} **(Ω.mg)**	42	65	28	43

4. Conclusion

$LiFePO_4$ (LFP) electrodes with two different LFP particle sizes were manufactured using a water-based process and xanthan gum (XG) as binder. The impact of both the particle size of the LFP and the electrode loading on the performance and stability of the electrodes was studied. Dramatic differences were observed between two different electrode groups made of LFP powders with different particle size distribution. Increased active material loading affects both electrode groups, especially at high C-rates, but differences are striking when the particle size distribution changes. While both electrode groups can hold their initial capacity at low C-rates (*e.g.* C/5), the results diverge for cycling rates of C and above. On the one hand, multiplying by 4 the LFP loading (from 3 to 12 mg on 1.88 cm^2 disc electrodes) has a significant impact on cells made of LFP with larger particles (0.84 µm); the capacity of those electrodes decreases almost by half at 2C. On the other hand, the capacity of the cells only decreases by about 30% at 2C when the particle size is decreased to 0.24 µm. The better rate capability of smaller LFP particles can be explained by the differences in charge transfer resistance, which is significantly lower when the particle size decrease. The difference of resistances results in performance modification, as observed in other works with classical electrodes manufactured using PVDF and NMP.

For the stability study, both groups were subjected to long-term cycling (100 cycles at C rate) and electrodes made of both LFP materials were affected by degradation. However, within the same group (*i.e.* same particle size), the capacity of cells with low loading (3 mg) was much less impacted than that of the cells with high loading (12 mg). While capacity retention was kept around 73% of its initial value for low loading, it can drop as low as 28% for high loading. In the meantime, cells prepared with smaller LFP particles gets much less degraded by long-term cycling. This phenomenon can be explained by Electrochemical Impedance Spectroscopy measurements. Indeed, one observes that both the interfacial and the charge transfer resistances, R_i and R_{ct}, increase for both LFP materials. However, the increase of R_i and R_{ct} upon cycling is less pronounced in the case of small LFP particles.

This work shows that, when considering manufacturing, one must take into account both the raw materials properties and the electrode design parameters such as its maximum thickness. Indeed, both are interrelated when considering the final electrode response to cycling. Depending on material and assembly costs and on the final battery use, one might adjust the electrode design to best fit the target. Finally, performance and phenomena observed were quite similar to those of polyvinylidene difluoride (PVDF)/ N-Methyl-2-pyrrolidone (NMP)-based electrodes and XG is thus confirmed to be a viable alternative to this classical toxic binder/solvent duo for LFP electrodes. Also, given the similarities between the two systems, observations done with the XG/water pair and related to the active material (*i.e.* particle size distribution) and electrode design (thickness) can be safely transposed to more classical electrodes made using the PVDF/NMP pair, even though the replacement of organic-based processing by water-based technique should be a priority in the very near future.

Acknowledgements

The authors would like to thank the F.R.S-FNRS for providing funding as part a PDR project (Convention T.0142.20). The authors also thank Prayon for providing P700 and P800 LFP samples.

REFERENCES

[1] N. Nitta, F. Wu, J.T. Lee, G. Yushin, Li-ion battery materials: Present and future, Mater Today 18 (2015) 252–264. https://doi.org/10.1016/j.mattod.2014.10.040.

[2] J.R. Dahn, E.W. Fuller, M. Obrovac, U. von Sacken, Thermal stability of Li_xCoO_2, Li_xNiO_2 and λ-MnO_2 and consequences for the safety of Li-ion cells, Solid State Ion 69 (1994) 265–270. https://doi.org/https://doi.org/10.1016/0167-2738(94)90415-4.

[3] A.K. Padhi, K.S. Nanjundaswamy, J.B. Goodenough, Phospho-olivines as positive-electrode materials for rechargeable lithium batteries, J Electrochem Soc 144 (1997) 1188–1194. https://doi.org/10.1149/1.1837571.

[4] W.J. Zhang, Structure and performance of $LiFePO_4$ cathode materials: A review, J Power Sources 196 (2011) 2962–2970. https://doi.org/10.1016/j.jpowsour.2010.11.113.

[5] H. Buqa, M. Holzapfel, F. Krumeich, C. Veit, P. Novák, Study of styrene butadiene rubber and sodium methyl cellulose as binder for negative electrodes in lithium-ion batteries, J Power Sources 161 (2006) 617–622. https://doi.org/10.1016/j.jpowsour.2006.03.073.

[6] A.F. Léonard, N. Job, Safe and green Li-ion batteries based on $LiFePO_4$ and $Li_4Ti_5O_{12}$ sprayed as aqueous slurries with xanthan gum as common binder, Mater Today Energy 12 (2019) 168–178. https://doi.org/10.1016/j.mtener.2019.01.008.

[7] A. F. Léonard, M.-L. Piedboeuf, N. Job. Process to prepare an electrode for an electrochemical storage device. EP16173423.1, June 7, 2016. WO2017211555A1.

[8] L. Bläubaum, F. Röder, C. Nowak, H.S. Chan, A. Kwade, U. Krewer, Impact of particle size distribution on performance of lithium-ion batteries, ChemElectroChem 7 (2020) 4755–4766. https://doi.org/10.1002/celc.202001249.

[9] A. Soloy, D. Flahaut, J. Allouche, D. Foix, G. Salvato Vallverdu, E. Suard, E. Dumont, L. Gal, F. Weill, L. Croguennec, Effect of particle size on $LiNi_{0.6}Mn_{0.2}Co_{0.2}O_2$ layered oxide performance in Li-ion batteries, ACS Appl Energy Mater 5 (2022), 5617-5632. https://doi.org/10.1021/acsaem.1c03924.

[10] N. Sinha, M. Nookala, The effect of particle size on performance of cathode materials of Li-ion batteries, J Indian Inst Sci 89 (2009) 381–392.

[11] R. Zhao, J. Liu, J. Gu, The effects of electrode thickness on the electrochemical and thermal characteristics of lithium ion battery, Appl Energy 139 (2015) 220–229. https://doi.org/10.1016/j.apenergy.2014.11.051.

[12] E.R. Logan, A. Eldesoky, Y. Liu, M. Lei, X. Yang, H. Hebecker, A. Luscombe, M.B. Johnson, J.R. Dahn, The effect of $LiFePO_4$ particle size and surface area on the performance of $LiFePO_4$/graphite cells, J Electrochem Soc 169 (2022) 050524. https://doi.org/10.1149/1945-7111/ac6aed.

[13] Y. Zhang, J.A. Alarco, J.Y. Nerkar, A.S. Best, G.A. Snook, P.C. Talbot, Improving the rate capability of $LiFePO_4$ electrode by controlling particle size distribution, J Electrochem Soc 166 (2019) A4128–A4135. https://doi.org/10.1149/2.0621916jes.

[14] I. D. A. Hamidah, A. Solehudin, A. Setiawan ,A. Hamdani, M. A. S. Hidayat, F. Adityawarman , F. Khoirunissa, A. B. D. Nandiyanto , Corrosion study of AISI 304 on KOH, NaOH, and NaCl solution as an electrode on electrolysis process. Journal of Engineering Science and Technology, 13(5) (2018) 1345-1351.

[15] S. Y. Li, B. C. Church, Effect of aqueous-based cathode slurry pH and immersion time on corrosion of aluminum current collector in lithium-ion batteries. Materials and Corrosion, 67(9) (2016) 978-987.

[16] Q. Zhao, Y. Zhang, Y. Meng, Y. Wang, J. Ou, Y. Guo, D. Xiao, Phytic acid derived $LiFePO_4$ beyond theoretical capacity as high-energy density cathode for lithium ion battery, Nano Energy 34 (2017) 408–420. https://doi.org/10.1016/j.nanoen.2017.03.006.

[17] Y.F. Pulido, C. Blanco, D. Anseán, M. González, J.C. Viera, V.M. García, Effect of aging on C/LFP battery impedance: Operating conditions to which the impedance has minimal variations, in: 2017 IEEE International Conference on Environment and Electrical Engineering and 2017 IEEE Industrial and Commercial Power Systems Europe (EEEIC / I&CPS Europe), 2017: pp. 1–5. https://doi.org/10.1109/EEEIC.2017.7977469.

[18] J. Jiang, W. Shi, J. Zheng, P. Zuo, J. Xiao, X. Chen, W. Xu, J.-G. Zhang, Optimized operating range for large-format $LiFePO_4$/graphite batteries, J Electrochem Soc 161 (2014) A336–A341. https://doi.org/10.1149/2.052403jes.

[19] W. Duan, M. Husain, Y. Li, N. ur R. Lashari, Y. Yang, C. Ma, Y. Zhao, X. Li, Enhanced charge transport properties of an LFP/C/graphite composite as a cathode material for aqueous rechargeable lithium batteries, RSC Adv 13 (2023) 25327–25333. https://doi.org/10.1039/D3RA04143C.

[20] J. P. Schmidt, T. Chrobak, M. Ender, J. Illig, D. Klotz, E. Ivers-Tiffée, Studies on LiFePO4 as cathode material using impedance spectroscopy. Journal of Power Sources, 196(12), (2011), 5342-5348.

[21] W. Choi, H.C. Shin, J.M. Kim, J.Y. Choi, W.S. Yoon, Modeling and applications of electrochemical impedance spectroscopy (EIS) for lithium-ion batteries, J Electrochem Sci Technol 11 (2020) 1–13. https://doi.org/10.33961/jecst.2019.00528.

[22] L. Wen, L. Wang, Z. Guan, X. Liu, M. Wei, D. Jiang, S. Zhang, Effect of composite conductive agent on internal resistance and performance of lithium iron phosphate batteries, Ionics 28 (2022) 3145–3153. https://doi.org/10.1007/s11581-022-04491-w.

[23] K.Y. Song, G.S. Jang, J. Tao, J.H. Lee, S.K. Joo, Effects of electrode thickness on three-dimensional NiCrAl metal foam cathode for lithium ion battery, J Nanosci Nanotechnol 18 (2017) 992–998. https://doi.org/10.1166/jnn.2018.13953.

[24] M.D. Murbach, V.W. Hu, D.T. Schwartz, Nonlinear electrochemical impedance spectroscopy of lithium-ion batteries: Experimental approach, analysis, and initial findings, J Electrochem Soc 165 (2018) A2758. https://doi.org/10.1149/2.0711811jes.

[25] J. Chidiac, L. Timperman, M. Anouti, Salt and solvent effect on physicochemical properties and species organisation of lithium fluorosulfonyl imide (FSI and TFSI) based electrolytes for Li-ion battery: Consequence on cyclability of $LiNi_{0.8}Co_{0.15}Al_{0.05}$ (NCA) cathode, J Taiwan Inst Chem Eng 126 (2021) 88–101. https://doi.org/10.1016/j.jtice.2021.06.049.

[26] H. Zheng, J. Li, X. Song, G. Liu, V.S. Battaglia, A comprehensive understanding of electrode thickness effects on the electrochemical performances of Li-ion battery cathodes, Electrochim Acta 71 (2012) 258–265. https://doi.org/10.1016/j.electacta.2012.03.161.

[27] K. Ariyoshi, M. Tanimoto, Y. Yamada, Impact of particle size of lithium manganese oxide on charge transfer resistance and contact resistance evaluated by electrochemical impedance analysis, Electrochim Acta 364 (2020) 137292. https://doi.org/10.1016/j.electacta.2020.137292.

[28] E. Teliz, C.F. Zinola, V. Díaz, Identification and quantification of ageing mechanisms in Li-ion batteries by electrochemical impedance spectroscopy, Electrochim Acta 426 (2022) 140801. https://doi.org/10.1016/j.electacta.2022.140801.

[29] J.M. Reniers, G. Mulder, D.A. Howey, Review and performance comparison of mechanical-chemical degradation models for lithium-ion batteries, J Electrochem Soc 166 (2019) A3189–A3200. https://doi.org/10.1149/2.0281914jes.

[30] Z. Zhou, Y. Liu, M. You, R. Xiong, X. Zhou, Two-stage aging trajectory prediction of LFP lithium-ion battery based on transfer learning with the cycle life prediction, Green Energy Intell. Transp. 1 (2022) 100008. https://doi.org/10.1016/j.geits.2022.100008.

[31] M. Ceraolo, G. Lutzemberger, D. Poli, C. Scarpelli, Experimental evaluation of aging indicators for lithium–iron–phosphate cells, Energies 14 (2021) 4813. https://doi.org/10.3390/en14164813.

[32] R. Scipioni, P.S. Jørgensen, D.I. Stroe, R. Younesi, S.B. Simonsen, P. Norby, J. Hjelm, S.H. Jensen, Complementary analyses of aging in a commercial $LiFePO_4$/graphite 26650 cell, Electrochim Acta 284 (2018) 454–468. https://doi.org/10.1016/j.electacta.2018.07.124.